Global and Planetary Change xxx (2012) xxx–xxx

Contents lists available at SciVerse ScienceDirect

Global and Planetary Change

journal homepage: www.elsevier.com/locate/gloplacha

Sensitivity of Late Permian climate to bathymetric features and implications for the mass extinction

Angela K. Osen *, Arne M.E. Winguth, Cornelia Winguth, Christopher R. Scotese

Department of Earth and Environmental Sciences, University of Texas at Arlington, 500 Yates Street, Arlington, TX 76019, USA

ARTICLE INFO

Article history:
Received 1 June 2011
Accepted 25 January 2012
Available online xxxx

Keywords:
Permian–Triassic boundary
mass extinctions
anoxia
ocean circulation
paleogeography
climate model

ABSTRACT

Evidence from stratigraphic sections of the Panthalassa, Paleo-Tethys and Neo-Tethys suggests that the oceans experienced widespread anoxia during the Late Permian, which likely contributed to the extinction of ~90% of marine and ~70% of terrestrial species. The Late Permian and Early Triassic were also characterized by significant carbon isotope excursions implying that considerable perturbations in the carbon cycle occurred. Bathymetric features of the Panthalassa during this period are not well known since most of the ocean floor has been subducted; however, tectonic reconstructions suggest that active marine subduction zones surrounded Pangea. Thus, it is reasonable to assume that there was an active mid-ocean ridge system located in Panthalassa during the Late Permian. In this study, the impact of such a spreading center within Panthalassa on the climate and carbon cycle is investigated using a comprehensive climate system model for the end-Permian. This is a novel approach because a majority of previous simulations assumed a flat bottom for the Panthalassa deep-sea. The mid-ocean ridge (MOR) simulation enhanced vertical mixing and topographic steering of the currents near the ridge-axis but in comparison with the simulation using a flat bottom, changes in the global distribution of water masses and circulation in the Panthalassa were insignificant. Dissolved oxygen concentrations were not considerably affected by the implementation of the mid-ocean ridge. Thus the approximation of using a flat-bottom topography in ocean models for the Late Permian remains valid.

In a second sensitivity study, the effect of a sill between the deep Paleo-Tethys and Panthalassa on water mass distribution and oxygen content has been investigated. Model results suggest that the introduction of a sill led to enhanced stratification, as well as an increase in salinity and temperature in the Paleo-Tethys. An associated reduction of the dissolved oxygen concentration to dysoxic to near-anoxic conditions below 1800 m suggests that the changes in sill height between the Paleo-Tethys and Panthalassa may have been a contributing factor of regional importance to the Permian-Triassic mass extinction.

1. Introduction

Near the Permian–Triassic boundary (approximately 252 Ma), the largest known mass extinction of the Phanerozoic occurred when more than 90% of all marine species and 70% of the terrestrial species became extinct (Erwin, 2006). Many hypotheses have been proposed concerning the causes of this extinction but the exact triggering mechanisms are still controversial. Outgassing from the Siberian Traps undoubtedly produced dramatic global warming due to a large influx of greenhouse gases into the atmosphere (Wignall, 2001; Reichow et al., 2009; Svensen et al., 2009), as inferred by climate-sensitive sediments (Royer, 2006; Breecker et al., 2010). One possible consequence of a CO_2-induced global warming is the enhancement of ocean stratification that can lead to widespread anoxia (Knoll et al., 1996; Meyer and Kump, 2008). While deep-sea anoxia has been inferred from pelagic sediments originating from the Panthalassa Ocean (Isozaki, 1997), modeling and recent geochemical studies suggest that the expansion of low-oxygen conditions occurred within the oxygen minimum zone rather than at the seafloor (Winguth and Maier-Reimer, 2005; Algeo et al., 2010; Winguth and Winguth, 2012). Geochemical data support the existence of dysoxic (~0.2–2 mL L^{-1} or ~5–45 μmol L^{-1}; Tyson and Pearson, 1991; Wignall et al., 2010) to anoxic (<0.2 mL L^{-1} or <5 μmol L^{-1}) water masses in the Tethys Ocean near the Permian–Triassic boundary (Newton et al., 2004; Grice et al., 2005; Cao et al., 2009).

A majority of modeling studies attempting to simulate oceanic conditions during the Late Permian have used uncoupled ocean general circulation models (OGCMs) (Hotinski et al., 2001; Zhang et al., 2001) or an energy balance model coupled with an OGCM (Winguth et al., 2002) in which forcings of temperature, freshwater and momentum fluxes are prescribed. Kiehl and Shields (2005) performed a fully coupled climate simulation that considered feedbacks between the different components of the climate system and more recently, Winguth and Winguth (2012) completed fully coupled climate–carbon cycle

* Corresponding author. Tel.:+1 817 272 5846.
E-mail addresses: angela.osen@mavs.uta.edu (A.K. Osen), awinguth@uta.edu (A.M.E. Winguth), cwinguth@uta.edu (C. Winguth), cscotese@uta.edu (C.R. Scotese).

0921-8181/$ – see front matter © 2012 Elsevier B.V. All rights reserved.
doi:10.1016/j.gloplacha.2012.01.011

simulations with and without an enhanced biological pump. However, these previous simulations featured a flat ocean bottom configuration with at least a partially open deep-water connection in the Tethys region. In order to fully determine the possible extent of anoxic conditions around the Permian–Triassic boundary, the paleobathymetric influences should be considered. For example, mid-ocean ridges can block deep-water currents as well as cause kinematic steering of flow about the ridge (Gille et al., 2004; Katsman, 2005; Thurnherr et al., 2011). Blockage of deep ocean basins may cause dense bottom waters to be redirected into downstream basins leading to stratification (Thurnherr et al., 2011). Isolation of basins by mid-ocean ridges, sills and/or shallow seas may restrict ventilation; however, enhanced mixing also occurs due to obstacles, particularly with the flow over rough topography (St. Laurent and Garrett, 2002; Jayne et al., 2003). Montenegro et al. (2011) inferred from climate simulations using an earth system model of intermediate complexity (EMIC) for the Permian–Triassic boundary with mid-ocean ridge bathymetries, that the meridional overturning circulation does not change significantly under consideration of a mid-ocean ridge. In this paper, the impacts of different bathymetric features (mid-ocean ridge in Panthalassa and sills between the Tethys and Panthalassa) on water mass distribution, ocean circulation, and oxygen distribution are explored with a more complex, fully coupled climate system model including a marine carbon cycle, in order to asses how environmental changes could have contributed to the mass extinction at the Permian-Triassic boundary.

2. Model description

2.1. Community Climate System Model (CCSM3)

The National Center for Atmospheric Research's Community Climate System Model 3 (CCSM3; Collins et al., 2006) was applied for the Late Permian sensitivity experiments described here (see Kiehl and Shields, 2005; Winguth and Winguth, 2012). The CCSM3 is a fully coupled model containing the four main components of the climate system (atmosphere, land, ocean, and sea-ice). Fluxes, boundary conditions, and physical state information are exchanged between the different components by a coupler (see Collins et al., 2006, and http://www.cesm.ucar.edu/models for more detailed information). For the atmospheric component, the Community Atmosphere Model version 3 (CAM3) was used with the spectral horizontal resolution grid T31 ($3.75°\times3.75°$) with 26 vertical levels (Collins et al., 2004, 2006). The drift within the global mean temperature at 4000 m is adjusting to the equilibrium and considered to be small (less than 0.01 °C per century and comparable to the modern control simulation of Yeager et al., 2006). The Community Land Model version 3 (CLM3.0) has a resolution of $2°\times2°$ (Oleson et al., 2004). CLM3.0 provides surface albedos, upward longwave radiation, sensible heat flux, latent heat flux, water vapor flux, as well as zonal and meridional surface stresses to the atmospheric model (Oleson et al., 2004). The ocean component consisted of the Parallel Ocean Program version 1.4 (POP), a general circulation model, in which three-dimensional primitive equations for ocean dynamics and a dipole grid with a nominal horizontal resolution of 3° and 25 vertical levels are used (Smith and Gent, 2004; Collins et al., 2006). The ocean module includes ideal age as a passive tracer used to measure the time (years) since a parcel of water has been transported away from the surface (England, 1995; Bryan et al., 2006; Kiehl, 2007). For the sea-ice component, a thermodynamic model, the Community Sea Ice Model version 5 (CSIM5; Briegleb et al., 2004; Collins et al., 2006) was used with the same horizontal and vertical resolution as in the ocean general circulation model.

2.2. Ocean carbon cycle

The CCSM3 in this version includes a carbon cycle model as described in Doney et al. (2006) and Winguth and Winguth (2012), which is based upon the Ocean Carbon Model Intercomparison Project (OCMIP-2) biotic carbon model of Najjar and Orr (1999; http://www.ipsl.jussieu.fr/OCMIP). Air–sea fluxes of CO_2 and oxygen were estimated using the wind-dependent gas exchange coefficient across the air-sea interface, along with partial pressures of CO_2 in the lower two layers of the atmosphere and the top layer of the ocean (Doney et al., 2006). The solubility of CO_2 and oxygen is temperature-dependent. The model includes five prognostic variables: inorganic phosphate, semilabile organic phosphorous, dissolved oxygen, dissolved inorganic carbon, and alkalinity (Doney et al., 2006; Najjar et al., 2007). The parameterization of biological uptake of nutrients assumes a constant Redfield ratio for particulate organic matter (Maier-Reimer, 1993). The uptake of PO_4 is given by the turnover of biomass, modulated by surface solar irradiance, and temperature, with phosphate and iron as the limiting nutrients within the model. Phosphate, generally well correlated to nitrate in the present ocean (Millero, 2006), was chosen as a limiting nutrient to reduce the computational costs associated with the complexities of nitrogen fixation and denitrification (Najjar and Orr, 1998). The model uses a Martin power–law curve ($a=-0.9$) to describe the vertical particulate organic phosphorus flux profile over the full water column. The flux is altered by scavenged Fe attached to the sinking matter throughout the water column (Doney et al., 2006).

2.3. Boundary conditions

Boundary conditions for all sensitivity experiments, including the reference (or control) experiment, were taken from the Kiehl and Shields (2005) CCSM3 simulation. The solar constant for the Permian-Triassic boundary is set to 1338 $W\,m^{-2}$, representing a 2.1% decrease from the modern value based upon calculations by Boothroyd (Caldeira and Kasting, 1992; Winguth et al., 2002). Eccentricity and the vernal equinox were set to zero, resulting in near equal receipt of solar insolation for both hemispheres (Gibbs et al., 2002). Earth's obliquity is set to 23.5°, equivalent to the modern value of the Earth's axial tilt. Greenhouse gas concentrations are taken from Kiehl and Shields (2005; see also Table 1) and are inferred from Kidder and Worsley (2004). The fixed land vegetation used in the experiments was adapted from the model simulation by Kiehl and Shields (2005) and based on paleo-vegetation models of Rees et al. (1999).

After the addition of the ocean carbon cycle to the 2700-year run by Kiehl and Shields (2005) with a flat bottom ocean configuration, the model was integrated for an additional 5300 years and served as the control experiment. The sensitivity experiments with a mid-ocean ridge (MOR) and with a sill between the Tethys and Panthalassa (hereafter named Tethys experiment) were initialized from the control simulation in year 5007 and integrated for 3000 years, corresponding to about three times the mean water mass residence time in Panthalassa.

2.4. Land–sea distribution

Land and sea configurations were taken from Kiehl and Shields (2005) for all experiments. As in the Kiehl and Shields (2005) simulation, the average depth of the ocean near the Permian–Triassic boundary is assumed to have been comparable with the mean depth of the present-day oceans and was therefore set to ~4 km. No changes were made to the control simulation that has a flat-bottom

Table 1
Boundary conditions for the Late Permian simulations. Table adapted from Kiehl and Shields (2005); ppmv is parts per million by volume.

	CO_2 (ppmv)	CH_4 (ppmv)	N_2O (ppmv)	S_0 (Wm^{-2})	Eccentricity	Obliquity
Value	3550	0.700	0.275	1338	0	23.5°

Please cite this article as: Osen, A.K., et al., Sensitivity of Late Permian climate to bathymetric features and implications for the mass extinction, Glob. Planet. Change (2012), doi:10.1016/j.gloplacha.2012.01.011

ocean configuration (Fig. 1A), while the bathymetry was modified for the MOR and Tethys experiments (Fig. 1B and C).

The MOR experiment included a mid-ocean ridge that extended across the Panthalassa Ocean in a general north–south direction (Fig. 1B). The position of the mid-ocean ridge was based on the assumption that the active subduction zones along the western margin of Pangea were supplied by a spreading center analogous to the East Pacific Rise. Like the modern East Pacific Rise, this ancient Panthalassic spreading center may have been oriented parallel to the subducting margins that surrounded Pangea. The fact that mid-ocean ridges tend to be aligned parallel to convergent boundaries has been noted by several authors (Forsyth and Uyeda, 1975; Scotese and Rowley, 1985). The mid-ocean ridge was assumed to be at least 21 million years old and to have a fast spreading rate of 10 cm yr^{-1}, which is comparable to the spreading rate of the present East Pacific Rise. The ocean floor was set at a maximum depth of 4007 m in the model, rendering the crest of the ridge at a depth of approximately 2800 m in the simulation. The estimation was loosely based on the formula from Stein and Stein (1992).

Table 2
Globally averaged ocean temperatures (°C).

	Surface	200 m	600 m	1100 m	1900 m	2800 m	3800 m
Control	22.66	16.52	10.89	7.16	5.72	5.11	4.85
MOR	22.65	16.47	10.90	7.26	5.82	5.20	4.89
Tethys	22.59	16.36	11.04	7.54	6.10	5.48	5.12

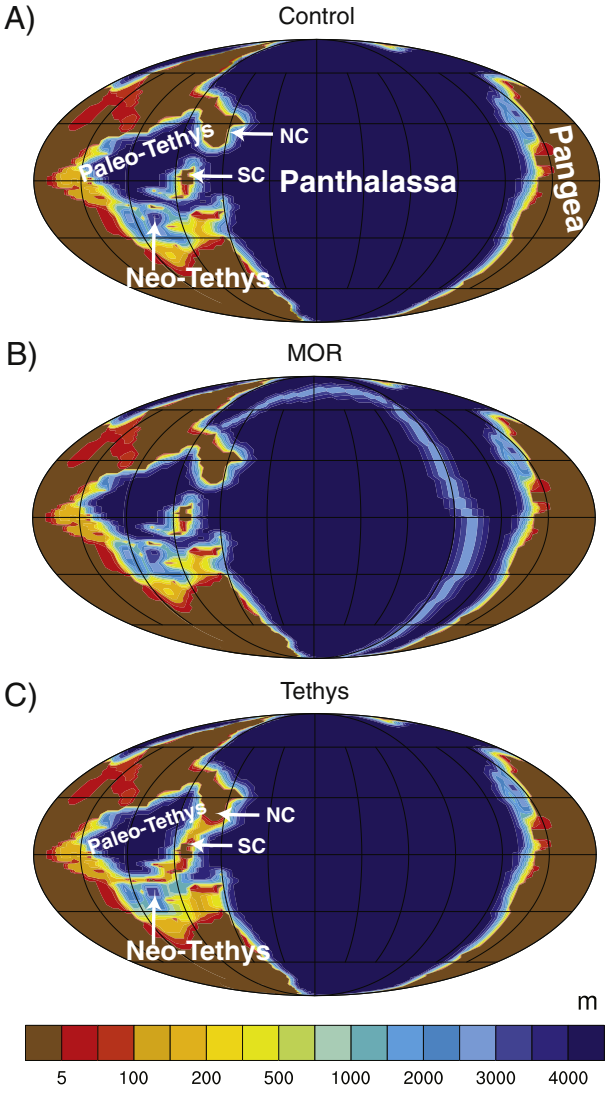

Fig. 1. Late Permian land–sea simulations for: (A) The control experiment, with a flat-bottom ocean and partially open exchange between the Paleo-Tethys, Neo-Tethys and Panthalassa Oceans. (B) The MOR experiment, with a mid-ocean ridge in the Panthalassa Ocean. (C) The Tethys experiment, with the addition of sills up to a depth of 200 m located at the eastern region of the Paleo-Tethys between the North China Block (NC) and South China (SC) section, including the Yangtze and Huanan blocks, and also in the southern Paleo-Tethys, separating the Paleo-Tethys from the Neo-Tethys Ocean.

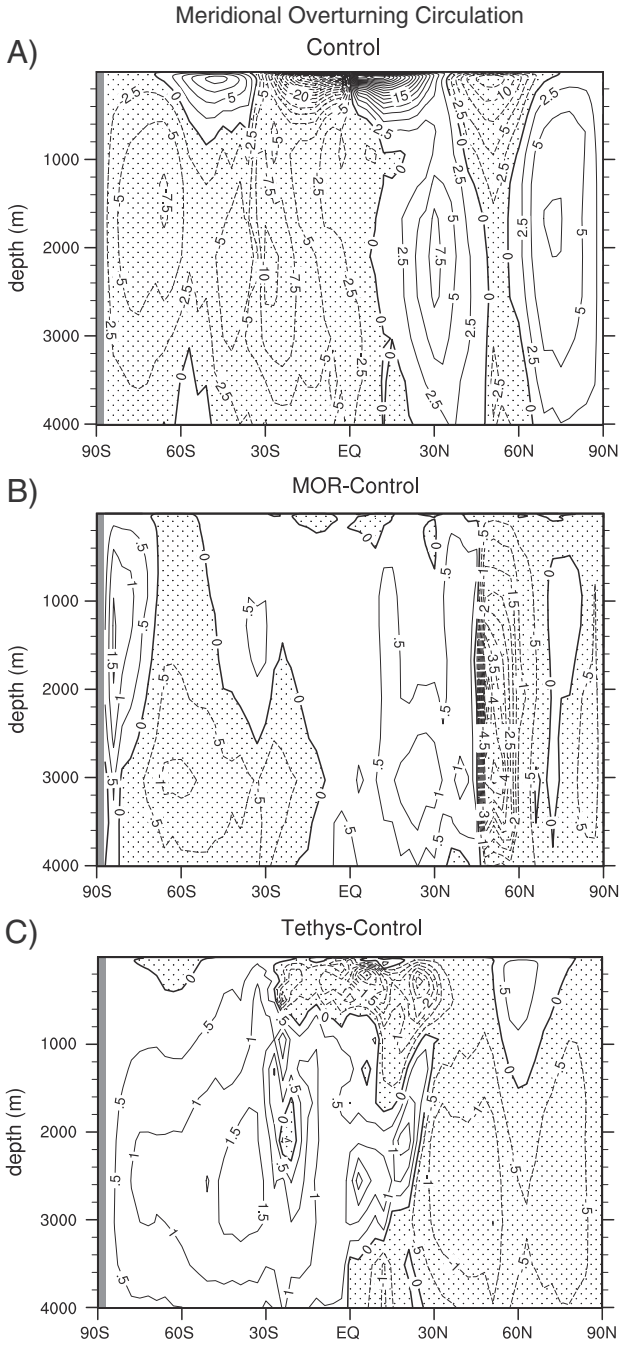

Fig. 2. Meridional overturning circulation in Sv (10^6 m^3 s^{-1}). (A) The control, shaded areas with negative values represent regions of downwelling and areas in white are regions of upwelling. (B) Change in the MOC between MOR and control simulations. Increased downwelling was simulated between 45°N and 60°N due to the addition of the mid-ocean ridge. Remaining ocean showed either no changes or slight decrease in overturning circulation. (C) Change in MOC between Tethys and control simulations. Decline of 0.5 to 1.5 Sv in the MOC was simulated throughout most of the Permian oceans.

Please cite this article as: Osen, A.K., et al., Sensitivity of Late Permian climate to bathymetric features and implications for the mass extinction, Glob. Planet. Change (2012), doi:10.1016/j.gloplacha.2012.01.011

However, the exact location of the Late Permian mid-ocean ridge remains uncertain because most of the seafloor has been subducted and other configurations like a Tethys–Panthalassa ridge-system as tested in Montenegro et al. (2011) or a tripod-shape may have been plausible.

The presence of a ridge disrupts normal deep-water flow resulting in internal waves that can lead to diapycnal mixing. The additional mixing can lead to horizontal density gradients, which can drive secondary flows (Thurnherr et al., 2011). Restriction of ocean circulation could conceivably alter the distribution of salinity and dissolved oxygen, as well as other elements. Changes of bathymetry might create additional mixing and upwelling of water masses and hence increase biological productivity (Hotinski et al., 2001; Winguth and Maier-Reimer, 2005). The effects of heat flow from the ridge or sea floor were neglected in all experiments.

The Tethys experiment included the addition of sills between the Paleo-Tethys and Panthalassa Oceans as well as the Paleo-Tethys and Neo-Tethys (without a mid-ocean ridge; Fig. 1C). The shallow sills effectively separated the Paleo-Tethys Ocean from the Panthalassa, restricting the water exchange between the two oceans below a depth of 200 m, whereas a deep passage between these oceans was present in the control and the MOR experiments. The modifications are based upon configurations from Scotese and Langford (1995). Paleomagnetic and geochronological data has been studied by many authors (e.g. Scotese and Langford, 1995; Zhao et al., 1996; Sengör and Atayman, 2009) and suggests that the collision of North and South China began

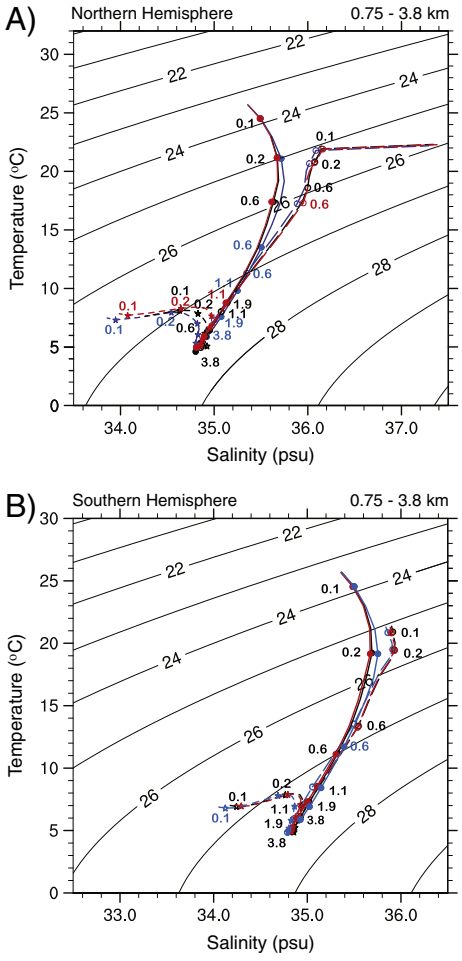

Fig. 3. Temperature–salinity diagram for Late Permian climate simulations with CCSM3 for the equator (solid line), 30° (long dash), and 60° (short dash) for the MOR experiment (red), Tethys experiment (blue) and the flat-bottom ocean floor control experiment (black). A) Northern Hemisphere and B) Southern Hemisphere. Dots denote the depth in km. (For interpretation of the references to color in this figure legend, the reader is referred to the web version of this article.)

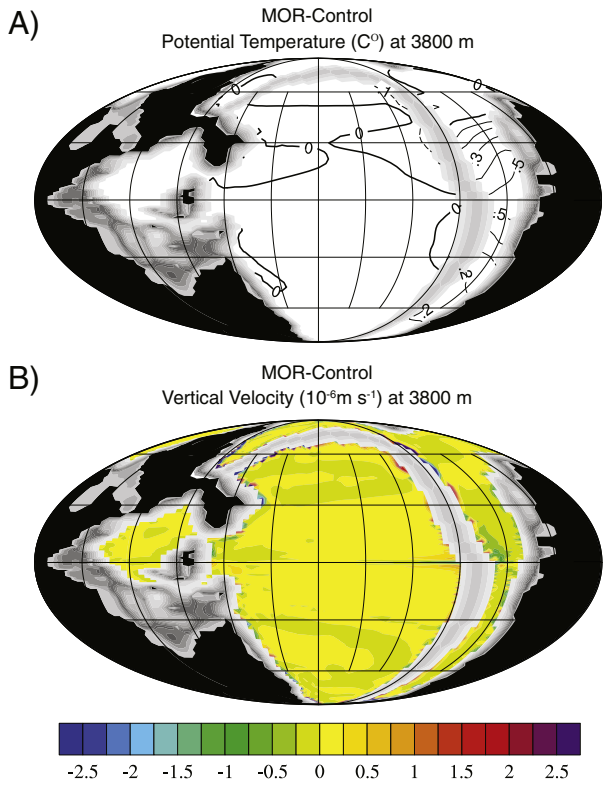

Fig. 4. At a depth of 3800 m, the difference between the MOR and control experiments in A) potential temperature (°C) and B) vertical velocity (10^{-6} m s^{-1}).

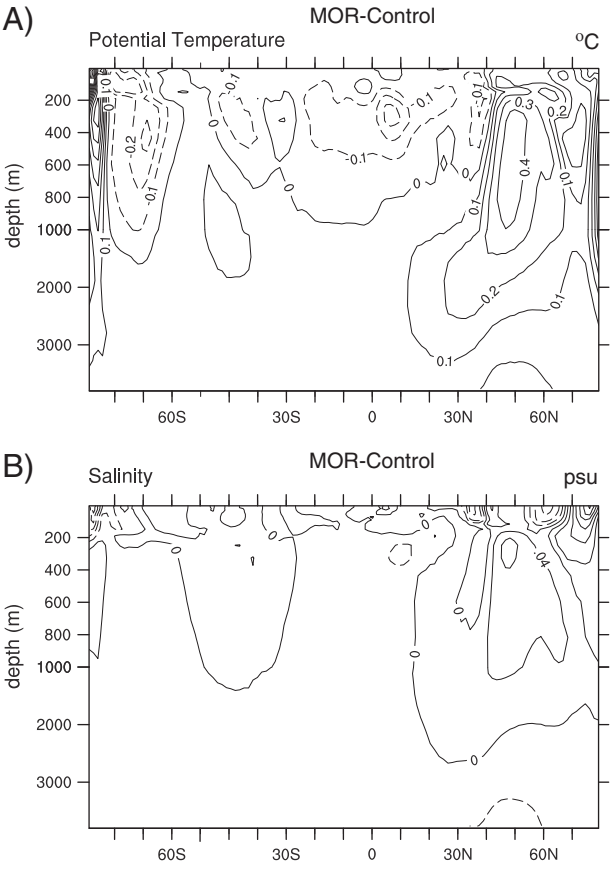

Fig. 5. Difference in global mean zonal averages between the MOR and control experiments in A) potential temperature (°C) and B) salinity (psu).

Please cite this article as: Osen, A.K., et al., Sensitivity of Late Permian climate to bathymetric features and implications for the mass extinction, Glob. Planet. Change (2012), doi:10.1016/j.gloplacha.2012.01.011

near the end of the Permian, but that these landmasses had not become completely sutured until the Mesozoic. However, there is no consensus on the extent of the oceanic passageway between the two blocks during the Late Permian. Results from Meng and Zhang (1999) proposed that a Paleo-Tethyan Ocean between the North and South China blocks existed and that subduction in this region may not have occurred until the Early Triassic. In contrast, Sengör and Atayman (2009) suggested the presence of a continental shelf basin (0–200 m) and possibly a land bridge, based on additional flora and fauna evidence, and that the isolation of the Paleo-Tethys might have contributed to the onset of oxygen-poor conditions in the region.

3. Results

3.1. Ocean circulation and water mass distribution

In the following, we discuss the physical and geochemical results of the MOR experiment and the Tethys experiment as compared to the control simulation. After 3000 years of model integration, a 100-year mean global average was computed for all three sensitivity experiments. The average sea surface temperature for all three sensitivity experiments was ~23 °C, while the temperature simulated for the deepest waters was approximately 5 °C (Table 2). Sea surface temperatures in the equatorial region were in the range of 26 °C to 32 °C for all experiments, while high-latitude (75°–90°) surface temperatures were in the range of 6 °C to 9 °C.

The major simulated sources of Late Permian deep-water masses are located at ~30° and in the polar region in both hemispheres (Figs. 2 and 3). The polar water mass is characterized by low temperature (4–6 °C) and salinity (34.6–34.8 psu), whereas the subtropical water mass can be identified by warmer, more saline characteristics with temperatures in the range of 14–16 °C and salinities of 35.3–35.5 psu. The latter is comparable with modern arid marginal seas like the Mediterranean Sea or the Red Sea. Away from the subtropical water formation areas near the east coast of Pangea, the thermocline is deeper than in the tropics because of the cooler sea surface temperature associated with the intertropical convergence zone and due to equatorial upwelling. In contrast to the present day, the deep-sea circulation is more symmetrical about the equator with a transport of ~8–10 Sv at 30° (Fig. 2A).

Differences in global large-scale ocean circulation patterns between the mid-ocean ridge and the flat-bottom simulations were small (as inferred from Figs. 2 and 3), but regional changes did occur, for example near 45°N, where deep-water transport increased by more than 4 Sv (Fig. 2B). Regional anomalies in temperature of

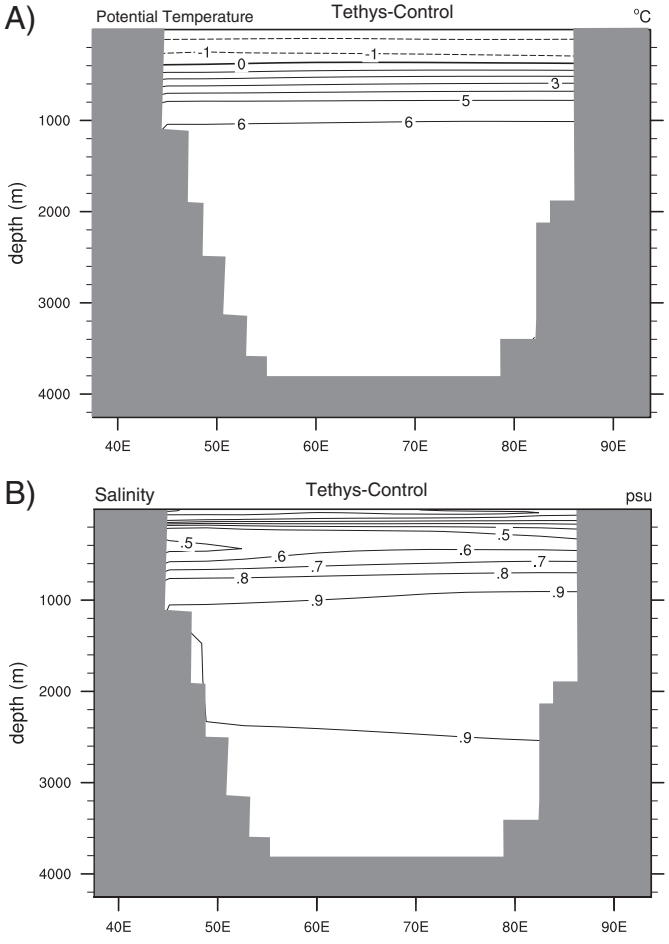

Fig. 6. Longitudinal section of the Tethys region about the equator of the difference between the Tethys and control experiments in A) potential temperature (°C) and B) salinity (psu).

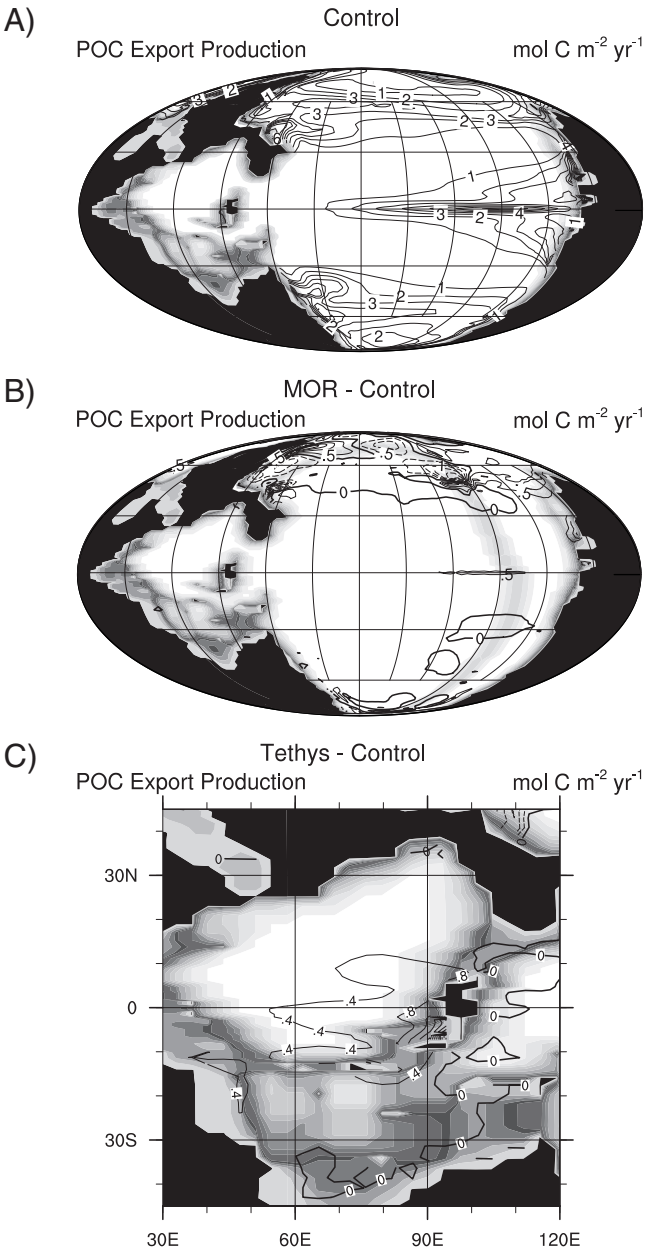

Fig. 7. A) Productivity in the control experiment (in mol C m^{-2} yr^{-1}), B) change in productivity between MOR and control experiments and C) difference in productivity in the Tethys region between the Tethys and control runs.

Please cite this article as: Osen, A.K., et al., Sensitivity of Late Permian climate to bathymetric features and implications for the mass extinction, Glob. Planet. Change (2012), doi:10.1016/j.gloplacha.2012.01.011

Table 3
Global particulate organic carbon export production.

Experiment name	100 year average ($Pg\ C\ yr^{-1}$)	Percent change
Control	8.03	–
MOR	8.43	4.98
Tethys	7.78	−3.11
Modern	6.73	−16.19

<2 °C and in salinity of <0.3 psu in the shallow-to-intermediate water masses were caused by topographic steering and enhanced vertical mixing due to the mid-ocean ridge, which acted like a barrier. However, changes in deep-sea temperatures (<0.5 °C; Fig. 4A) and salinities (not shown) were insignificant and confined to the region east of the mid-ocean ridge. Below 2000 m, the vertical velocities increased (Fig. 4B) due to topographic steering of the currents and increased mixing of the deep sea caused by the mid-ocean ridge. Circulation patterns within the deepest water masses were altered by the mid-ocean ridge, but these changes did not have a significant impact on the global mean temperature and salinity distribution, as shown in Fig. 5.

Temperature and salinity changes in the Tethys sensitivity experiment were largely confined to the Paleo-Tethys Ocean basin located about the equator. The exchange between Panthalassa and the Paleo-Tethys was disrupted by the reduction of the passage depth to 200 m that prevented the inflow of cooler deep-sea water masses from the Panthalassa to the Paleo-Tethys Ocean. Due to the stronger influence of subtropical deepwater formation near Northern China, the temperature and salinity of intermediate water masses below 1000 m near the equator rose by up to 6 °C (Fig. 6A) and 0.9 psu (Fig. 6B), respectively. The isolation of the Paleo-Tethys Ocean allows for stratification of the water masses and is comparable to the layering in the present-day Mediterranean Sea. The distribution of water masses and the meridional overturning circulation in the Panthalassa and Neo-Tethys Oceans were not significantly affected by the sill (Fig. 2C).

3.2. Productivity, dissolved oxygen and ideal age of water masses

3.2.1. Productivity

The simulated export production depends on macro- and micronutrient availability, temperature, and light availability. Significant nutrient uptake occurs in upwelling areas and zones of a deep mixed-layer depth. For example, in the control experiment production is greatest in the coastal regions and near the equator (Fig. 7A). The simulated Late Permian productivity in the control simulation is 16.19% lower than the modern productivity simulated by CCSM3 (Table 3). Compared to the control simulation, the MOR simulation increased by 4.98% (Table 3 and Fig. 7B) due to enhanced vertical mixing (Fig. 4B). The greatest gains in productivity occurred between 15°N and 50°N in the Panthalassa Ocean off the coast of Pangea and near the northwestern costal region of Pangea between 60°N and 80°N (Fig. 7B).

The average global export production decreased by 3.11% in the Tethys experiment compared to the control run (Table 3). However, the addition of the sills to the Tethys led to increased upwelling and enhanced productivity in the southern region of the Paleo-Tethys (Fig. 7C).

3.2.2. Dissolved oxygen and ideal age of water masses

The ideal age of the water masses (Fig. 8A) acts as a passive circulation tracer, with low age values representing a well-mixed environment and high values a sluggish circulation with longer residence times in the deep-sea. The distribution of dissolved oxygen concentrations in the deep-sea generally follows the distribution of the idealized age tracer (Fig. 8B), but also depends on the local productivity (Fig. 7A).

Enhanced mixing caused by the mid-ocean ridge increased dissolved oxygen concentrations within deep waters. Upwelling in regions east of the mid-ocean ridge (Fig. 4B) is reflected in the ideal age of the water masses in the western Panthalassa (Fig. 8C) and contributed to increased dissolved oxygen concentrations of up to 50.0 $\mu mol\ L^{-1}$ at 3800 m (Fig. 8D).

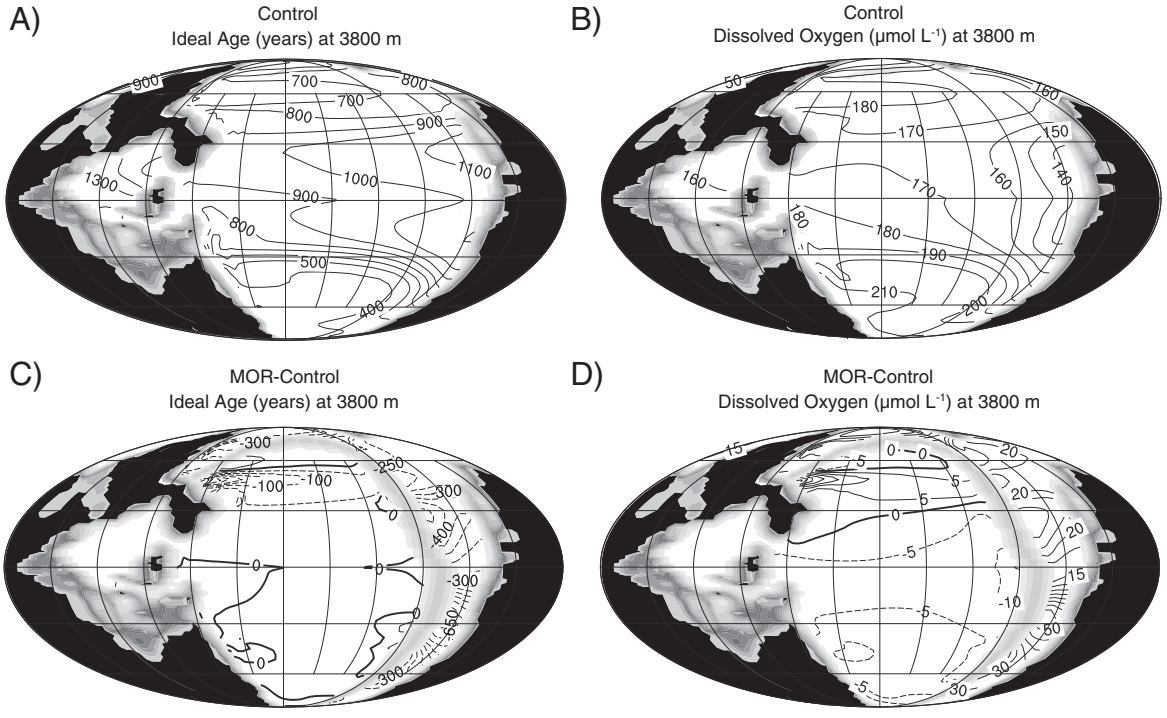

Fig. 8. Simulations for the control at 3800 m for (A) ideal age of water masses in years and (B) dissolved oxygen concentration in $\mu mol\ L^{-1}$. Difference between MOR and control experiments at 3800 m for C) ideal age of water masses in years and D) dissolved oxygen concentration in $\mu mol\ L^{-1}$.

Please cite this article as: Osen, A.K., et al., Sensitivity of Late Permian climate to bathymetric features and implications for the mass extinction, Glob. Planet. Change (2012), doi:10.1016/j.gloplacha.2012.01.011

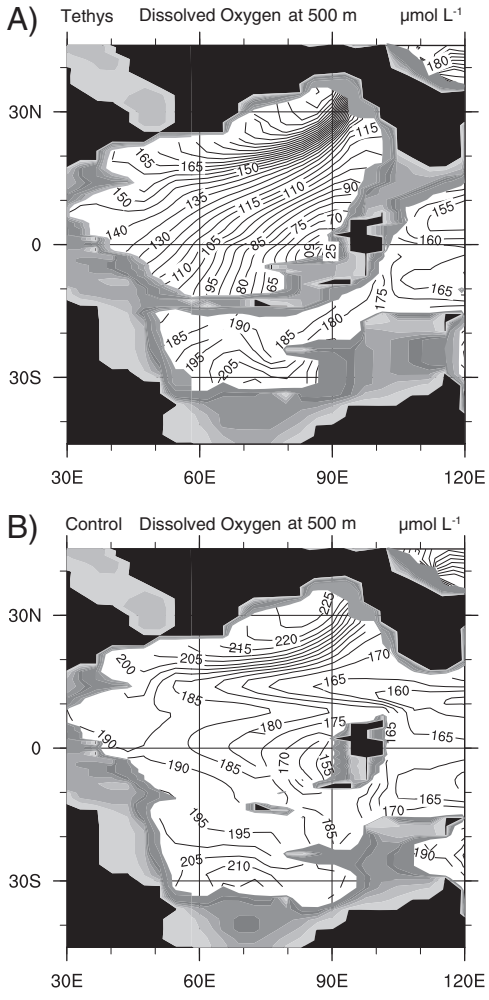

Fig. 9. Dissolved oxygen concentrations in the Tethys region at 500 m for A) Tethys and B) control experiments.

Differences in dissolved oxygen between the Tethys simulation with sills and the control simulation with a deep passage are related to the warming anomaly (Fig. 6A) and associated stratification as well as positive productivity fluctuation along the equatorial region of the southeastern Paleo-Tethys (Fig. 7C). At an intermediate depth of 500 m, oxygen gradients increased remarkably with the closure of the deeper Paleo-Tethys. An oxygen minimum zone with dissolved oxygen concentrations as low as 25 µmol L^{-1} developed along the eastern shores of the Paleo-Tethys (Fig. 9A) that was not simulated in the control experiment (Fig. 9B) because of slightly enhanced equatorial productivity along with the blocking of well-ventilated water masses from Panthalassa and from the Neo-Tethys. The idealized age of water masses at 3300 m for the control experiment ranged from 1100 to 1500 years in the Paleo-Tethys basin (Fig. 10A). The Tethys experiment revealed an increase in stagnation with the deep sea increasing in age by 1700 to 2000 years compared to the control experiment, with the Paleo-Tethys having an absolute ideal age of approximately 3100 years (Fig. 10B). Horizontal velocities within the Paleo-Tethys basin at 3300 m decreased from the control experiment (Fig. 10A) and were less than 0.05 cm s^{-1} (Fig. 10B). The sluggish circulation coupled with the lack of deep-water exchange between the Paleo-Tethys and Panthalassa as well as increased oxygen demand from enhanced productivity resulted in greatly reduced oxygen concentrations within the Paleo-Tethys (Fig. 11) and to a lesser extent within the Panthalassa (not shown). The equatorial cross-section of dissolved oxygen concentrations within the Paleo-Tethys suggests that the dissolved oxygen concentration decreased by more than 120 µmol L^{-1} (Fig. 11), yielding dysoxic conditions below 1800 m (Fig. 11B).

4. Discussion

The addition of the mid-ocean ridge did not change the meridional overturning circulation significantly (Fig. 3.) However, as shown in Fig. 4B, upwelling in the ultimate vicinity of the ridge increased, which reduced the ideal age of water masses and increased dissolved oxygen concentrations due to a slightly higher influence of warm and saline subtropical water masses in areas located east of the ridge. The deep sea at 3800 m depth remained well oxygenated in the MOR simulation (Fig. 8B and D). The control and MOR experiments did not simulate anoxic conditions in the Tethys region where the majority of euxinic to anoxic sedimentary evidence from the Permian-Triassic boundary has been identified (Sengör and Atayman, 2009). Furthermore, deep-sea anoxia was not simulated in the Panthalassa and Tethys oceans with the present-day nutrient inventory, contrary to suggestions by Hotinski et al. (2001) and by Kiehl and Shields (2005) who inferred anoxia from higher-than-present-day water mass stratification during the Late Permian in their CCSM3 simulation

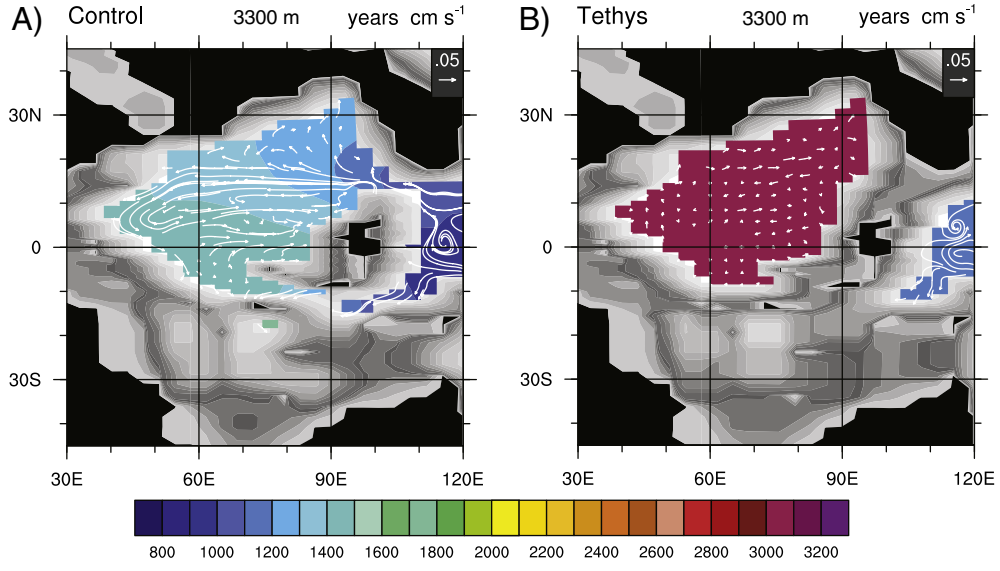

Fig. 10. Ideal age (years) of water masses and horizontal velocities (cm s^{-1}) at 3300 m for A) the control and B) the Tethys experiments.

Please cite this article as: Osen, A.K., et al., Sensitivity of Late Permian climate to bathymetric features and implications for the mass extinction, Glob. Planet. Change (2012), doi:10.1016/j.gloplacha.2012.01.011

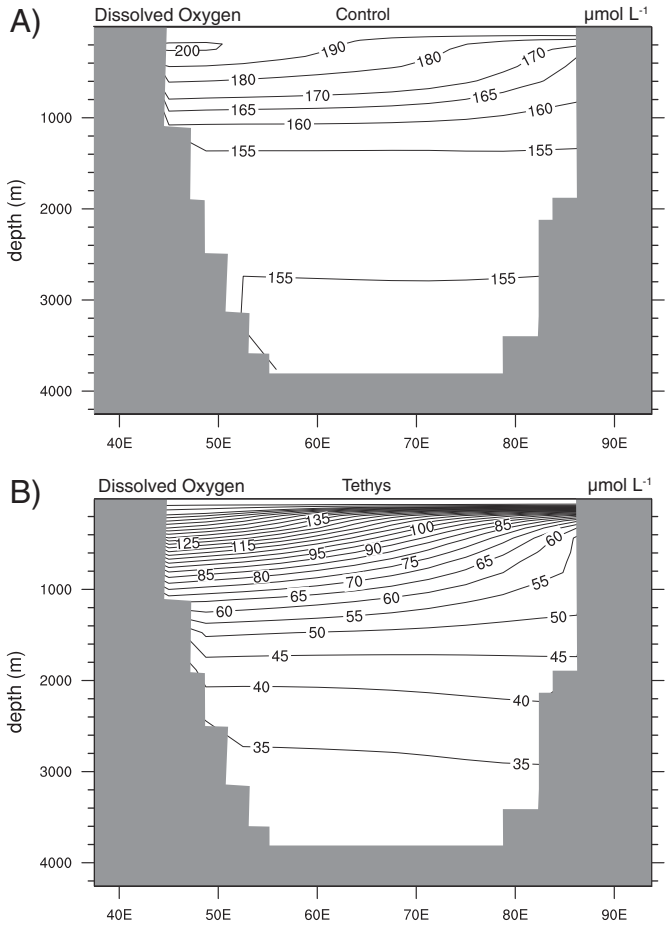

Fig. 11. Longitudinal section of the Tethys region about the equator of dissolved oxygen concentrations (μmol L^{-1}) for A) control and B) Tethys experiments.

results without an ocean carbon cycle model. However, the findings of this study that the deep Panthalassa and Tethys are not anoxic (with dissolved oxygen concentrations >120 μmol L^{-1}) are consistent with Montenegro et al. (2011) who conducted sensitivity experiments using an earth system model of intermediate complexity featuring 2 mid-ocean ridge configurations (one in which a straight ridge was placed directly through the middle of the Panthalassa Ocean in a north–south direction and a second in which the mid-ocean ridge traverses through the Paleo-Tethys and becomes a U-shaped ridge within the Panthalassa). Additionally, Meyer and Kump (2008), Meyer et al. (2008), and Winguth and Winguth (2012) suggested a high sensitivity of the deep-sea oxygen concentration to changes in the nutrient inventory and enhanced biological pump.

The closure of the Paleo-Tethys region in the Tethys sensitivity experiment by a sill generated stratified water masses within the basin, associated with an increase in the ideal age of deep-water masses, and led to a decline in dissolved oxygen concentrations within the Paleo-Tethys basin to dysoxic conditions (Fig. 11B). Sengör and Atayman (2009) suggest that a combination of atmospheric, lithospheric and biospheric changes in the Paleo-Tethys contributed to the anoxic conditions in the latest Permian. Dysoxic conditions along the eastern inner shores of the Tethys region within the oxygen minimum zone are supported by evidence of Chlorobiaceae (green sulfur bacteria), a biomarker indicator of anoxygenic photosynthesis, in the Meishan section, South China (Grice et al., 2005; Cao et al., 2009) as well as pyrite formation (Jiang et al., 2006). Indicators of an oxygen-restricted environment are also present in Northern Xinjang, China (Cao et al., 2008). Permian–Triassic sections in South China suggest an increase in salinity that may have been induced by rising temperatures and evaporation rates (Chai et al., 1992), which is in agreement with the Tethys sensitivity experiment. Dysoxic conditions were not modeled for the western shores of the Paleo-Tethys region, conflicting with geological evidence inferring anoxia in the Siusi section of Northern Italy (Wignall and Twitchett, 1996; Newton et al., 2004); however, dysoxic conditions were simulated in the deep-sea. The difference could be related to the coarse resolution of the model not resolving coastal process, or uncertainties in the prediction of coastal winds influencing the buoyancy forcing and Ekman-upwelling.

All sensitivity experiments do have some limitations that are summarized in the following: (1) Low resolution was used in all experiments that limits the representation of bathymetric features such as seamounts, small islands or trenches which could further influence oceanic circulation. Topographic roughness of mid-ocean ridges can increase the strength of internal tides (St. Laurent and Garrett, 2002), which cannot be resolved using low-resolution models. (2) The sulfur cycle was not included in any of the simulations. With the long-term eruptions of the Siberian Traps occurring during the Late Permian, large amounts of sulfur dioxide would have been released into the atmosphere (Reichow et al., 2002; Heydari et al., 2008; Saunders and Reichow, 2009) that would have been converted to sulfuric acid and increased weathering and erosion rates. (3) Sediment and silicate cycles were not included in the experiments, which may have influenced productivity and ocean chemistry. Geological evidence suggests that an increase in erosion may have played a role in the deterioration of oceanic conditions (Wang and Visscher, 2007; Algeo and Twitchett, 2010; Algeo et al., 2011).

5. Conclusions

The placement of a mid-ocean ridge within Panthalassa had only a minor impact on the global water mass distribution and oceanic conditions. Thus the flat-bottom approach in ocean models for the Late Permian remains a valid approximation. Increased upwelling in the vicinity of the ridge due to topographic steering redirected flows about the ridge but did not significantly change temperature and salinity distributions within the Panthalassa.

The introduction of a sill between the North and South China blocks induced a decrease of circulation and enhanced stratification within the Paleo-Tethys, led to the development of dysoxic conditions in the region. Global currents and meridional overturning circulation were impacted to a much smaller extent. For an isolated Paleo-Tethys, deteriorated environmental conditions with warm temperatures and low oxygen would have contributed to the regional extinction of species; however, these changes would probably not have been sufficient to explain the global marine mass extinction.

Acknowledgments

We thank Christine Shields and Jeff Kiehl at the National Center for Atmospheric Research (NCAR) for providing the initial boundary conditions for the simulations and technical support. We thank T. Algeo, L. Kump, Y. Isozaki and an anonymous reviewer for their insightful suggestions on the manuscript. All model simulations were done on NCAR computers, supported by NSF. The work is supported by NSF Grant EAR-0745817.

References

Algeo, T., Twitchett, R., 2010. Anomalous Early Triassic sediment fluxes due to due to elevated weathering rates and their biological consequences. Geology 38, 1023–1026.
Algeo, T.J., Hinnov, L., Moser, J., Maynard, J.B., Elswick, E., Kuwahara, K., Sano, H., 2010. Changes in productivity and redox conditions in the Panthalassic Ocean during the latest Permian. Geology 38 (2), 187–190.
Algeo, T.J., Chen, Z.Q., Fraiser, M.L., Twitchett, R.J., 2011. Terrestrial–marine teleconnections in the collapse and rebuilding of Early Triassic marine ecosystems. Palaeogeography, Palaeoclimatology, Palaeoecology 308, 1–11.

Breecker, D.O., Sharp, Z.D., McFadden, L.D., 2010. Atmospheric CO_2 concentrations during ancient greenhouse climates were similar to those predicted for A.D. 2100. PNAS 107 (2), 576–580.
Briegleb, B.P., Bitz, C.M., Hunke, E.C., Lipscomb, W.H., Holland, M.M., Schramm, J.L., Schramm, Moritz, R.E., 2004. Scientific description of the sea ice component in the Community Climate System Model, Version Three. Tech. Rep. NCAR/TN-463+STR, National Center for Atmospheric Research, Boulder, CO. 78 pp.
Bryan, F.O., Danbasoglu, G., Nakashiki, N., Yoshida, Y., Kim, D.-H., Tsutsui, J., Doney, S.C., 2006. Response of the North Atlantic thermohaline circulation and ventilation to increasing carbon dioxide in CCSM3. Journal of Climate 19, 2382–2397.
Caldeira, K., Kasting, J.F., 1992. The life span of the biosphere revised. Nature 360, 721–723.
Cao, C., Wang, W., Liu, L., Shen, S., Summons, R.E., 2008. Two episodes of ^{13}C-depletion in organic carbon in the latest Permian: evidence from the terrestrial sequences in northern Xinjiang, China. Earth and Planetary Science Letters 270, 251–257.
Cao, C., Love, G.D., Hays, L.E., Wang, W., Shen, S., Summons, R.E., 2009. Biogeochemical evidence for euxinic oceans and ecological disturbance presaging the end-Permian mass extinction event. Earth and Planetary Science Letters 281, 188–201.
Chai, C., Zhou, Y., Mao, X., Ma, S., Ma, J., Kong, P., He, J., 1992. Geochemical constraints on the Permo-Triassic boundary event in South China. In: Sweet, W.C., Zunyi, Y., Dickins, J.M., Hongfu, Y. (Eds.), Permo-Triassic Events in the Eastern Tethys: Stratigraphy, Classification, and Relations with the Western Tethys. Cambridge University Press, UK, pp. 158–168.
Collins, W.D., Bitz, C.M., Blackmon, M.L., Bonan, G.B., Bretherton, C.S., Carton, J.A., Chang, P., Boney, S.C., Hack, J.J., Henderson, T.B., Diehl, J.T., Large, W.G., McKenna, D.S., Santer, B.D., Smith, R.D., 2004. Description of the NCAR Community Atmosphere Model (CAM3). Tech. Rep. NCAR/TN-464+STR, National Center for Atmospheric Research, Boulder, CO. 226 pp.
Collins, W.D., Bitz, C.M., Blackmon, M.L., Bonan, G.B., Bretherton, C.S., Carton, J.A., Chang, P., Boney, S.C., Hack, J.J., Henderson, T.B., Diehl, J.T., Large, W.G., McKenna, D.S., Santer, B.D., Smith, R.D., 2006. The Community Climate System Model Version 3 (CCSM3). Journal of Climate 19, 2122–2143.
Doney, S.C., Lindsay, K., Fung, I., John, J., 2006. Variability in a stable, 1000-yr global coupled climate–carbon cycle simulation. Journal of Climate 19, 3033–3054.
England, M.H., 1995. The age of water and ventilation timescales in a global ocean model. Journal of Physical Oceanography 25, 2756–2777.
Erwin, D.H., 2006. Extinction: How Life on Earth Nearly Ended 250 Million Years Ago. Princeton University Press, Princeton, New Jersey. 296 pp.
Forsyth, D., Uyeda, S., 1975. On the relative importance of the driving forces of plate motion. Geophysical Journal of the Royal Astronomical Society 43, 163–200.
Gibbs, M.T., Rees, P.M., Kutzbach, J.E., Ziegler, A.M., Behling, P.J., Rowley, D.B., 2002. Simulations of Permian climate and comparisons with climate-sensitive sediments. Journal of Geology 110, 33–55.
Gille, S.T., Metzger, E.J., Tokmakian, R., 2004. Seafloor topography and ocean circulations. Oceanography 17, 47–54.
Grice, K., Cao, C., Love, G.D., Böttcher, M.E., Twitchett, R.J., Grosjean, E., Summons, R.E., Turgeon, S.C., Dunning, W., Jin, Y., 2005. Photic zone euxinia during the Permian–Triassic superanoxic event. Science 307, 706–709.
Heydari, E., Arzani, N., Hassanzadeh, J., 2008. Mantle plume: the invisible serial killer — application to the Permian–Triassic boundary mass extinction. Palaeogeography, Palaeoclimatology, Palaeoecology 264, 147–162.
Hotinski, R.M., Bice, K.L., Kump, L.R., Najjar, R.G., Arthur, M.A., 2001. Ocean stagnation and end-Permian anoxia. Geology 29 (1), 7–10.
Isozaki, Y., 1997. Permo-Triassic boundary superanoxia and stratified superocean: from lost deep sea. Science 276 (5310), 235–238.
Jayne, S.R., St. Laurent, L.C., Gille, S.T., 2003. Connections between ocean bottom topography and Earth's climate. Oceanography 17 (1), 65–74.
Jiang, Y.F., Tang, Y.G., Chou, C.L., 2006. Research on genesis of pyrite near the Permian–Triassic boundary in Meishan, Zhejiang, China. China University of Mining and Technology 16 (4), 457–460.
Katsman, C.A., 2005. Impacts of localized mixing and topography on the stationary abyssal circulation. Journal of Physical Oceanography 36, 1660–1671.
Kidder, D.L., Worsley, T.R., 2004. Causes and consequences of extreme Permo-Triassic warming to globally equable climate and relation to the Permo-Triassic extinction and recovery. Palaeogeography, Palaeoclimatology, Palaeoecology 203, 207–237.
Kiehl, J.T., 2007. Modelling the climates of the Late Paleozoic. Deep-time perspectives on climate change: marrying the signal from computer models and biological proxies. In: Williams, M., Haywood, A.M., Gregory, F.J., Schmidt, D.N. (Eds.), The Micropalaeontological Society. Special Publications, Geological Society of London, pp. 157–167.
Kiehl, J.T., Shields, C.A., 2005. Climate simulation of the latest Permian: implications for mass extinction. Geology 33 (9), 757–760.
Knoll, A.H., Bambach, R.K., Canfield, D.E., Grotzinger, J.P., 1996. Comparative Earth history and Late Permian mass extinction. Science 273, 452–457.
Maier-Reimer, E., 1993. Geochemical cycles in an ocean general circulation model. Preindustrial tracer distributions. Global Biogeochemical Cycles 7 (3), 645–677.
Meng, Q.-R., Zhang, G.-W., 1999. Timing of collision of the North and South China blocks: controversy and reconciliation. Geology 27 (2), 123–126.
Meyer, K.M., Kump, L.R., 2008. Oceanic euxinia in Earth history: causes and consequences. Annual Review of Earth and Planetary Sciences 36, 251–288.
Meyer, K.M., Kump, L.R., Ridgwell, A., 2008. Biogeochemical controls on photic-zone euxina during the end-Permian mass extinction. Geology 36, 747–750.
Millero, F.J., 2006. Chemical Oceanography, 3rd ed. CRC Press, Boca Raton, FL. 496 pp.
Montenegro, A., Spence, P., Meissner, K.J., Eby, M., Melchin, M.J., Johnston, S.T., 2011. Climate simulations of the Permian–Triassic boundary: ocean acidification and the extinction event. Paleoceoanography 26 (3207), 1–19.
Najjar, R., Orr, J., 1998. Design of OCMIP-2 simulations of chlorofluorocarbons, the solubility pump and common biogeochemistry. http://www.ipsl.jussieu.fr/OCMIP/phase2/simulations/design.ps. 18 Mar. 2011.
Najjar, R.G., Orr, J.C., 1999. Biotic-HOWTO. http://www.ipsl.jussieu.fr/OCMIP/. 18 Mar. 2011.
Najjar, R.G., Jin, X., Louanchi, F., Aumont, O., Caldeira, K., Doney, S.C., Dutay, J.-C., Follows, M., Gruber, N., Joos, F., Lindsay, K., Maier-Reimer, E., Matear, R.J., Matsumoto, K., Monfray, P., Mouchet, A., Orr, J.C., Plattner, G.-K., Sarmiento, J.L., Schlitzer, R., Slater, R.D., Weirig, M.-F., Yamanaka, Y., Yool, A., 2007. Impact of circulation on export production, dissolved organic matter, and dissolved oxygen in the ocean: results from phase II of the Ocean Carbon–cycle Model Intercomparison Project (OCMIP-2). Global Biogeochemical Cycles 21 (3007), 1–22.
Newton, R.J., Pevitt, E.L., Wignall, P.B., Bottrell, S.H., 2004. Large shifts in the isotopic composition of seawater sulphate across the Permo-Triassic boundary in northern Italy. Earth and Planetary Science Letters 218, 331–345.
Oleson, K.W., Bitz, C.M., Blackmon, M.L., Bonan, G.B., Bretherton, C.S., Carton, J.A., Chang, P., Boney, S.C., Hack, J.J., Henderson, T.B., Diehl, J.T., Large, W.G., McKenna, D.S., Santer, B.D., Smith, R.D., 2004. Technical description of the Community Land Model (CLM). Tech. Rep. NCAR/TN-461+STR, National Center for Atmospheric Research, Boulder, CO. 174 pp.
Rees, P.M., Gibbs, M.T., Ziegler, A.M., Kutzbach, J.E., Behling, P.J., 1999. Permian climates: evaluating model predictions using global paleobotanical data. Geology 27, 891–894.
Reichow, M.K., Saunders, A.D., White, R.V., Pringle, M.S., Al'Mukhamedov, A.I., Medvedev, A.I., Kirda, N.P., 2002. $^{40}Ar/^{39}Ar$ dates from the west Siberian basin: Siberian flood basalt province doubled. Science 296, 1846–1849.
Reichow, M.K., Pringle, M.S., Al'Mukhamedov, A.I., Allen, M.B., Andrechev, V.L., Buslov, M.M., Daivies, C.E., Fedoseev, G.S., Fitton, J.G., Inger, S., Medvedev, A.Ya., Mitchell, C., Puchkov, V.N., Safonova, I.Yu., Scott, R.A., Saunders, A.D., 2009. The time and extent of the eruption of the Siberial Traps large igneous province: implications for the end-Permian environmental crisis. Earth and Planetary Science Letters 277, 9–20.
Royer, D.L., 2006. CO_2-forced climate thresholds during the Phanerozoic. Geochimica et Cosmochimica Acta 70, 5665–5675.
Saunders, A., Reichow, M., 2009. The Siberian traps and the end-Permian mass extinction: a critical review. Chinese Science Bulletin 54 (1), 20–37.
Scotese, C.R., Langford, R.P., 1995. Pangea and the paleogeography of the Permian. In: Scholle, P.A., Peryt, T.M., Ulmer-Scholle, D.S. (Eds.), The Permian of Northern Pangea. Paleogeography, Paleoclimates, and Stratigraphy, vol. 1. Springer, Berlin, pp. 3–19.
Scotese, C.R., Rowley, D.B., 1985. The orthogonality of subduction: an empirical rule? Tectonophysics 116, 173–187.
Sengör, A.M.C., Atayman, S., 2009. The Permian extinction and the Tethys: an exercise in global geology: Geol. Soc. Spec. Pub., 448, pp. 1–85.
Smith, R., Gent, P. (Eds.), 2004. Reference manual for the Parallel Ocean Program (POP) ocean component of the Community Climate System Model (CCSM2.0 and 3.0): Tech. Rep. LA-UR-02-2484, Los Alamos National Laboratory and National Center for Atmospheric Research. Available online at http://www.cesm.ucar.edu/models/ccsm3.0/pop/doc/POPusers_main.html.
Stein, C.A., Stein, S., 1992. A model for the global variation in oceanic depth and heat flow with lithospheric age. Nature 359, 123–129.
St. Laurent, L., Garrett, C., 2002. The role of internal tides in mixing the deep ocean. Journal of Physical Oceanography 32, 2882–2899.
Svensen, H., Planke, S., Plozov, A.G., Schmidbauer, N., Corfu, F., Podladchikov, Y.Y., Jamtveit, B., 2009. Siberia gas venting and the end-Permian environmental crisis. Earth and Planetary Science Letters 277, 490–500.
Thurnherr, A.M., Ledwell, J.R., Lavelle, J.W., Mullineaux, L.S., 2011. Topography and circulation near the crest of the East Pacific Rise between 9° and 10°N. Deep Sea Research I 58, 365–376.
Tyson, R.V., Pearson, T.H., 1991. Modern and ancient continental shelf anoxia: an overview: Geol. Soc. London Spec. Pub., 58, pp. 1–24.
Wang, C., Visscher, H., 2007. Abundance anomalies of aromatic biomarkers in the Permian–Triassic boundary section at Meishan, China — evidence of end-Permian terrestrial ecosystem collapse. Palaeogeography, Palaeoclimatology, Palaeoecology 252, 291–303.
Wignall, P.B., 2001. Large igneous provinces and mass extinctions. Earth-Science Reviews 53, 1–33.
Wignall, P.B., Twitchett, R.J., 1996. Oceanic anoxia and the end Permian mass extinction. Science 272, 1155–1158.
Wignall, P.B., Bond, D.P.G., Kuwahara, K., Kakuwa, Y., Newton, R.J., Poulton, S.W., 2010. An 80 million year oceanic redox history from Permian to Jurassic pelagic sediments of the Mino-Tamba terrane, SW Japan, and the origin of four mass extinctions. Global and Planetary Change 71, 109–123.
Winguth, A.M.E., Maier-Reimer, E., 2005. Causes of marine productivity and oxygen changes associated with the Permian–Triassic boundary: a reevaluation with ocean general circulation models. Marine Geology 217, 283–304.
Winguth, A.M.E., Heinze, C., Kutzbach, J.E., Maier-Reimer, E., Mikolajewicz, U., Rowley, D., Rees, A., Ziegler, A.M., 2002. Simulated warm polar currents during the Middle Permian. Palaeocenography 17 (4), 1057, doi:10.1029/2001PA000646.
Winguth, C., Winguth, A.M.E., 2012. Simulating Permian–Triassic oceanic anoxia distribution: implications for species extinction and recovery. Geology 40, 127–130. doi:10.1130/G32453.1.
Yeager, S.G., Shields, C.A., Large, W.G., Hack, J.J., 2006. The low-resolution CCSM3. Journal of Climate 19, 2545–2566.
Zhang, R., Follows, M.J., Grotzinger, J.P., Marshall, J., 2001. Could the Late Permian deep ocean have been anoxic? Paleoceanography 16 (3), 317–329.
Zhao, X., Coe, R.S., Gilder, S.A., Frost, G.M., 1996. Palaeomagnetic constraints on the palaeogeography of China: implications for Gondwanaland. Australian Journal of Earth Sciences 43 (6), 643–672.

Please cite this article as: Osen, A.K., et al., Sensitivity of Late Permian climate to bathymetric features and implications for the mass extinction, Glob. Planet. Change (2012), doi:10.1016/j.gloplacha.2012.01.011